11-2010

Fabrication and Characterization of Coupled Metal-Dielectric-Metal Nanoantennas

Bhuwan Joshi
Kent State University - Kent Campus

Xuejin Wen

Kai Sun

Wu Lu

Qi-Huo Wei
Kent State University - Kent Campus, qwei@kent.edu

Fabrication and characterization of coupled metal-dielectric-metal nanoantennas

Bhuwan Joshi
Liquid Crystal Institute, Kent State University, Kent, Ohio 44242

Xuejin Wen
Department of Electrical and Computer Engineering, Ohio State University, Columbus, Ohio 43210

Kai Sun
Department of Material Science and Engineering, University of Michigan, Ann Arbor, Michigan 48109

Wu Lu[a)]
Department of Electrical and Computer Engineering, Ohio State University, Columbus, Ohio 43210

Qi-Huo Wei[b)]
Liquid Crystal Institute, Kent State University, Kent, Ohio 44242

(Received 9 July 2010; accepted 7 September 2010; published 10 November 2010)

The authors fabricated two dimensional arrays of metal-dielectric-metal nanoantennas consisting of a thin layer of light-emitting polymers sandwiched between two Ag parallel cuboids and characterized them by measuring the optical transmission through the antenna arrays. The measured transmission spectra show two resonant dips. Numerical simulations reproduce the experimental results and show that the left dip is due to a cavity resonance mode and the right dip is due to the absorption of the polymer. With this vertical antenna design, the dielectric gap can be made much smaller with an extremely small mode volume, making it a potential candidate for single molecule studies using surface enhanced Raman scattering and for various other optoelectronic applications. © *2010 American Vacuum Society.* [DOI: 10.1116/1.3501349]

I. INTRODUCTION

Considerable recent attention has been attracted by plasmonics in controlling and manipulating surface plasmon waves at the dielectric-metal interfaces[1] because of their potential applications in a myriad of applications.[2–4] One particular area of interest is related to confining or focusing electromagnetic waves into nanometer sizes or mode volumes.[5] The large wave vector or small wavelength of surface plasmons makes it possible to confine electromagnetic waves to dimensions much smaller than their wavelength in vacuum. Highly focused local field can lead to extraordinary effects and device applications such as nonlinear optical effects,[6] enhanced fluorescence[7] and Raman emission,[8,9] and miniaturized optical devices with exceptional properties.[4,10]

In order to achieve efficient focusing, plasmonic nanoantennas of various shapes such as metallic tips,[11–13] bow ties,[14] nanodisk,[15] and nanorod dimers (two rods separated by a small distance)[16–18] have been introduced and studied. It has been shown that the maximal local field enhancements are confined at the nanogaps between nanoparticle dimers.[19] In addition to these horizontal designs, vertical nanoantennas composed of metal-dielectric-metal components have also been introduced.[20–22] In those vertical nanoantennas, since the dielectric gap can be controlled precisely by advanced deposition methods such as atomic layer deposition, the antenna resonance and the plasmonic nanocavity resonance can be precisely tuned and shows promise for large scale manufacturing. For example, Miyazaki and Kurokawa showed in experiments that light can be squeezed into rectangular metal-dielectric-metal nanocavities of 3 nm thickness,[23] and Qin *et al.* demonstrated that metal-dielectric-metal (MDM) nanoantennas can be synthesized by using the so called on-wire lithography, a technique in which nanowires of different metal materials are alternatively electrochemically deposited in porous alumina templates with desired pore diameters and the final MDM nanoantennas are obtained by chemically remove the template and the middle metal material to form nanogaps.[24]

Recently, we studied the MDM plasmonic nanoantennas made of two different geometric shapes: parallel cuboids and cylinders.[25,26] Large local field enhancements have been observed when the antenna and cavity resonant frequencies are fine tuned. Narrow-band resonant peaks can be clearly seen in local field enhancement spectra; at the same positions of these local field peaks, dips can be observed in the far-field transmission or scattering spectra. It is understood that these local field peaks and far-field dips are due to resonant cavity modes inside the dielectric gaps formed by interfering gap plasmons. The tunability of the gap size with high accuracy makes this kind of nanoantenna design a good candidate for studies of single molecule SERS.

In this article, we present the fabrication and characterization of two dimensional (2D) arrays of MDM nanoantennas composed of a thin layer of light-emitting polymers sandwiched between two metal nanoparticles. We study the cavity resonance of these nanostructures by measuring the opti-

a)Electronic mail: lu@ece.osu.edu
b)Electronic mail: qwei@kent.edu

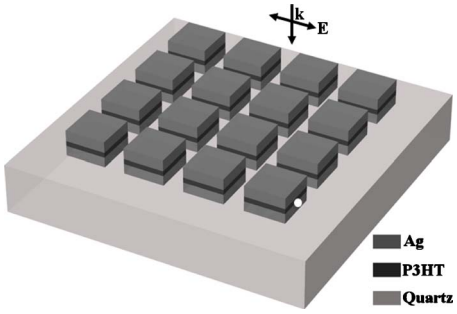

FIG. 1. Schematic Ag/P3HT/Ag nanoantenna array.

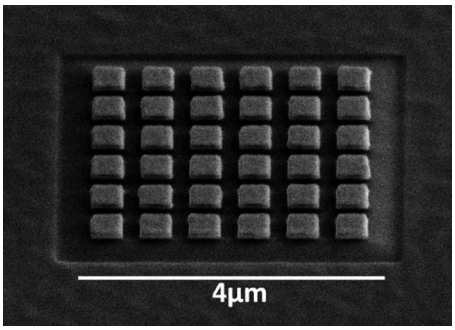

FIG. 2. Representative SEM image of a 2D array of fabricated Ag/P3HT/Ag nanoantennas. For this particular case, the side width of the cuboids is 420 nm.

cal transmission through the antenna arrays. We observed two resonant dips in the optical transmission spectra: The first dip position at about 450 nm shifts to red when the lateral size of these nanoantennas is increased, and the second dip exhibits very little change with the variation in antenna sizes. We performed numerical simulations by using finite-difference time domain algorithms, and we were able to reproduce those transmission dips in the calculated transmission spectra. Simulation results show that the first dip in the transmission spectra corresponds to a peak in local field enhancement spectra, and at the frequency of the second transmission dip, the calculated local field shows no enhancements. We attribute the first transmission dip to a coupled plasmonic nanocavity mode and the second transmission dip to the absorption of the polymers.

Incorporating the active materials inside the nanocavities of a very small mode volume and fine-tuning the cavity resonance to match with the active material's optical emission peak, the nanocavities can be potentially used in lasing application.

II. NANOANTENNA FABRICATION

A schematic representation of the MDM nanoantennas is shown in Fig. 1. The 2D arrays of the MDM nanoantennas are composed of a thin layer of light-emitting conjugated polymer 3-polyhexothyophene (P3HT) sandwiched between two silver (Ag) cuboids. To fabricate these nanoantennas, the first layer of Ag film was deposited on a quartz substrate using e-beam evaporation, and then a thin layer of P3HT was coated on this Ag film by spin-coating P3HT dissolved in chloroform at a spin speed of 3000 rpm, followed by baking on a hotplate at 95 °C for 5 min. After that, a second layer of Ag film was deposited through e-beam evaporation. 2D arrays of cuboid MDM nanoantennas were fabricated using focused ion beam milling (FEI Nova Nanolab). For better control over the nanoantenna dimension and to reduce the fabrication time, two steps were followed in the focused ion beam milling process. In the first step, a 30 kV Ga^+ beam with a 50 pA beam current was used to make a large trench around the area where nanoantenna arrays were to be fabricated. The unmilled area in the middle of the trench was milled by the ion beam with a smaller beam current (10 pA) to form the nanoantenna arrays.

To control the thickness of P3HTs films, its dependence on various physical parameters was studied and calibrated. Chloroform solutions of P3HT at different concentrations were spin-coated on clean silicon substrates at different spin speeds, and their film thicknesses were measured by an atomic force microscope. It was observed that the film thickness depends primarily on the concentration and has little variation with the spin speed. For a concentration of 1.38 mg/ml, the P3HT film is about 10 nm thick, while for a concentration of 2.9 mg/ml, the P3HT film is 20 nm thick.

For the data presented in this article, the thickness of the P3HT layer used is 20 nm; the thicknesses of the bottom and top Ag cuboids are 40 and 50 nm, respectively. The side width of nanoantennas is varied from 300 to 420 nm, and the array period was fixed at 600 nm. As an example, the scanning electron microscope (SEM) image of a 2D array of the fabricated nanoantennas is shown in Fig. 2.

III. RESULTS

We measured the optical transmission through the fabricated 2D arrays of Ag/P3HT/Ag nanoantennas. For the measurements, the nanoantenna arrays were illuminated perpendicularly with a collimated white light beam from the top, with a polarization parallel to the side widths of the nanoantennas. The transmitted light was collected by using a 40× objective with a 0.6 numerical aperture. The measured transmission spectra are presented in Fig. 3. Two dips can be observed from the transmission spectra. Both dips show a distinctive redshift in the dip wavelength when the side width of the nanoantennas is increased. One interesting observation is that with the same amount of increase in side width, the left dip shifts about twice as much in the wavelength as the right dip.

To understand the origin of these resonant dips, we performed numerical simulations using a commercial software package (CST MICROWAVE STUDIO). The CST software employs the finite integration technique and is considered a generalization of the finite-difference time domain method. The Drude dispersion model, $\varepsilon_{\mathrm{Ag}}=\varepsilon_\infty-\omega_p^2/\omega(\omega+i\gamma)$, was used to describe the Ag permittivity, where the parameters $\varepsilon_\infty=3.57$, $\omega_p=1.388\times10^{16}$ rad/s, and $\gamma=1.064\times10^{14}$ Hz were obtained by fitting the model with previous experimental

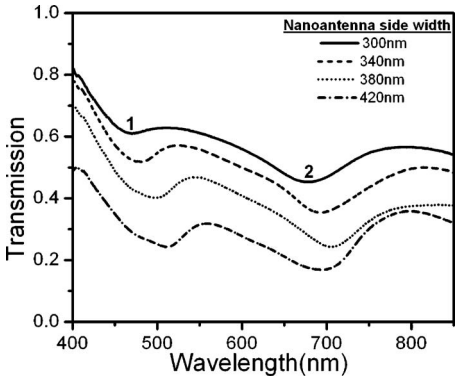

FIG. 3. Measured transmission spectra for the 2D arrays of Ag/P3HT/Ag with the side width at 300, 340, 380, and 420 nm.

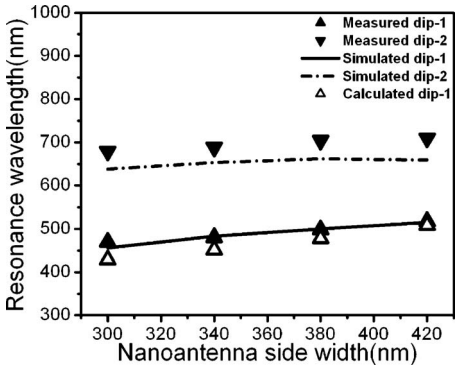

FIG. 5. Comparison of dip wavelengths vs nanoantenna side width obtained from the experimental, simulation, and analytical resonant condition results.

data.[27] To describe the permittivity of the P3HT, the general second order dispersion model, $\varepsilon(\omega)=\varepsilon_\infty+(\beta_0+i\omega\beta_1)/(\alpha_0+i\omega\alpha_1-\omega^2)$, was used, where the parameters $\varepsilon_\infty=2.5$, $\alpha_0=4.26\times10^{32}$ (rad/s)^2, $\alpha_1=4.14\times10^{15}$ rad/s, $\beta_0=1.87\times10^{32}$ (rad/s)^2, and $\beta_1=3.71\times10^{15}$ rad/s were obtained by fitting the model with the previously measured refractive index of the P3HT.[28] A glass substrate with a thickness of 550 nm and a permittivity of 2.13 was also used in the simulations. A plane polarized light wave was used to illuminate the nanoantennas from the top, with its electric field parallel to one side of the nanoantennas (shown in Fig. 1). The hexahedral meshing scheme was used, with the mesh size set much smaller than the wavelength of the surface plasmons ($\sim\lambda/35$). Transmission spectra were calculated by integrating the Poynting vectors at a plane that is 500 nm below the nanoantennas and inside the glass substrate. The optical transmission through the substrate with nanoantennas was normalized by the transmission through a bare substrate.

The simulated transmission spectra [Fig. 4(a)], which show two distinctive dips, are in close agreement with the experimental results, as can also be seen from the comparison of dip wavelengths in Fig. 5. We also calculated the spectra for the local electrical field at the middle point in the cavity edge, as indicated by the white spot in Fig. 1. Clear local field enhancement peaks are observed at the wavelengths of the left dips, indicating that the left dip corresponds to resonant excitation of a cavity mode inside the nanocavities. In contrast, the near-field spectra do not show any peaks at the positions of the right dips, indicating that the dips do not originate from cavity resonances. Considering the absorption and emission of the P3HT polymers at around 600 nm, the right dip can be attributed to the permittivity variations of the polymer.

The electric field distributions in the middle plane of the nanocavities at the corresponding wavelengths of these dips were calculated. Representative snapshots of the electric field distributions are shown in Figs. 6(a) and 6(b). The black and white colors represent the respective maxima and minima of the electric field. At the cavity resonance (the left dip), it can be observed that the electric fields form standing waves along the polarization direction (i.e., vertical direction) [Fig. 6(a)] and that the electrical fields form varying or propagating waves in horizontal directions. For the local field distribution corresponding to the right dip, the interference patterns vary in time in both vertical and horizontal directions, indicating no standing wave formation [Fig. 6(b)].

Based on previous studies, plasmonic cavity resonances are formed by the interfering gap plasmons confined between

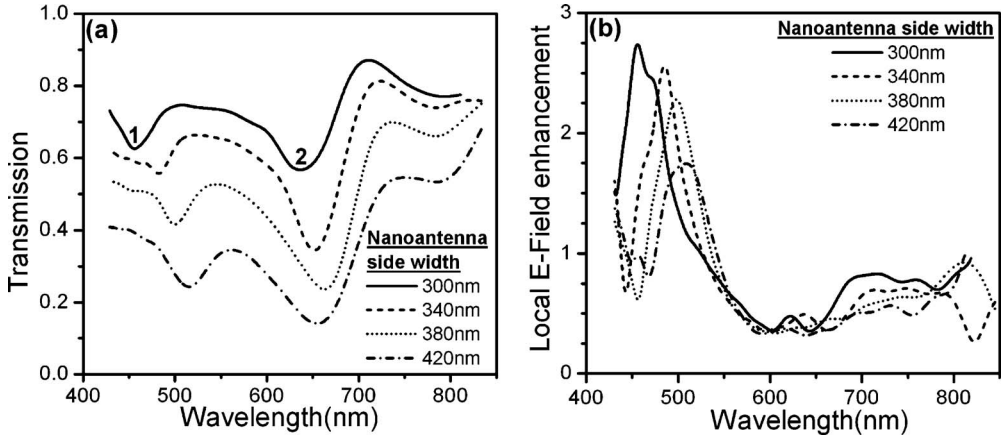

FIG. 4. (a) Simulated transmission spectra and (b) local electric field enhancement spectra for the 2D arrays of Ag/P3HT/Ag nanoantennas.

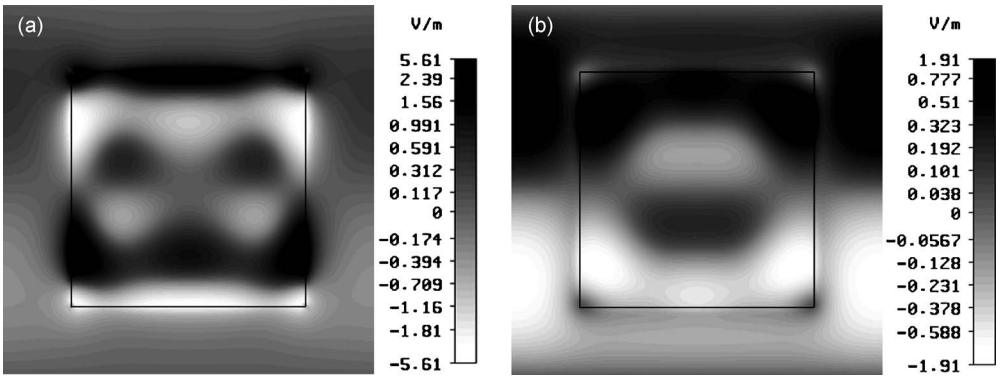

FIG. 6. Local electric field distribution at the middle plane inside the nanocavities corresponding to (a) dip 1 and (b) dip 2 of the transmission spectra. The electric field distributions presented here are for the nanoantenna arrays with 380 nm side widths.

two metal surfaces. The dispersion relation of the surface plasmon mode at a semi-infinite metal-dielectric interface is given by $k_{sp}=(\omega/c)\sqrt{\varepsilon_m\varepsilon_d/(\varepsilon_m+\varepsilon_d)}$, where ε_m and ε_d are the permittivities of the metal and dielectric materials, respectively, and ω and c are the radial frequency and speed of the electromagnetic waves in vacuum. In a MDM type of structures, the surface plasmon coupling between two close metal/dielectric interfaces causes the splitting of the single surface plasmon mode into two (symmetric and antisymmetric).[21,29] The symmetric mode has higher energy than the antisymmetric mode and is ignored here. Dispersion relation for the antisymmetric mode is given by

$$\tanh(k_d t/2) = -\varepsilon_d k_m/\varepsilon_m k_d, \quad (1)$$

where t is the dielectric gap thickness, $k_m=\sqrt{k_{gsp}^2-\varepsilon_m\omega^2/c^2}$, and $k_d=\sqrt{k_{gsp}^2-\varepsilon_d\omega^2/c^2}$. As a result of constructive interference between incident and reflected gap plasmon waves, the antinode is always formed at the edge. The resonance condition for isolated plasmonic nanocavities can be expressed as

$$k_{gsp}L = (2n+1)\pi, \quad n = 0,1,2,3\ldots, \quad (2)$$

where k_{gsp} is the gap plasmon wave vector[29] of the antisymmetric mode and can be calculated using Eq. (1) and L is the side width of the nanocavity. The integer $2n+1$ represents the number of antinodes formed by the interfering surface plasmon waves. The local field distributions show that $n=2$ for the left resonance dip. A comparison of the resonance wavelength obtained from experiments and simulations and calculated from Eq. (2) is shown in Fig. 5. The good agreement is achieved between calculated, experimental, and numerical results.

IV. SUMMARY

In conclusion, we have fabricated 2D arrays of plasmonic nanoantennas, which are composed of a thin layer of conjugated polymer sandwiched between two metal cuboids. We experimentally and numerically studied the optical transmission of nanoantennas arrays and numerically calculated their local field spectra. It is shown that for the nanoantennas with a conjugated polymer gap, cavity resonance modes can be excited. The cavity resonance modes produce dips in the transmission spectra and peaks in the local electric fields. The cavity resonance modes and their wavelengths vary systematically with the size of the nanoantennas at a constant gap size.

ACKNOWLEDGMENTS

This project was supported by the Ohio Board of Regents through a research challenge grant and by the National Science Foundation (Grant Nos. ECCS-0954976 and ECCS-0824175).

[1]H. Raether, Springer Tracts Mod. Phys. **111**, 1 (1988).
[2]J. Homola, S. S. Yee, and G. Gauglitz, Sens. Actuators B **54**, 3 (1999).
[3]W. L. Barnes, A. Dereux, and T. W. Ebbesen, Nature (London) **424**, 824 (2003).
[4]J. A. Schuller, E. S. Barnard, W. Cai, Y. C. Jun, J. S. White, and M. L. Brongersma, Nature Mater. **9**, 193 (2010).
[5]S. Maier, Opt. Quantum Electron. **38**, 257 (2006).
[6]V. M. Shalaev, *Nonlinear Optics of Random Media: Fractal Composites and Metal Dielectric Films* (Springer, Berlin, 2000), Vol. V158, p. 1–157.
[7]J. R. Lakowicz, Anal. Biochem. **337**, 171 (2005).
[8]K. Kneipp, H. Kneipp, I. Itzkan, R. R. Dasari, and M. S. Feld, Chem. Rev. (Washington, D.C.) **99**, 2957 (1999).
[9]A. Campion and P. Kambhampati, Chem. Soc. Rev. **27**, 241 (1998).
[10]E. Ozbay, Science **311**, 189 (2006).
[11]D. K. Gramotnev and K. C. Vernon, Appl. Phys. B: Lasers Opt. **86**, 7 (2007).
[12]A. L. Demming, F. Festy, and D. Richards, J. Chem. Phys. **122**, 184716 (2005).
[13]J. Kim, G. L. Liu, Y. Lu, and L. P. Lee, Opt. Express **13**, 8332 (2005).
[14]P. J. Schuck, D. P. Fromm, A. Sundaramurthy, G. S. Kino, and W. E. Moerner, Phys. Rev. Lett. **94**, 017402 (2005).
[15]K. H. Su, Q. H. Wei, X. Zhang, J. J. Mock, D. R. Smith, and S. Schultz, Nano Lett. **3**, 1087 (2003).
[16]P. K. Jain, S. Eustis, and M. A. El-Sayed, J. Phys. Chem. B **110**, 18243 (2006).
[17]P. Pramod and K. G. Thomas, Adv. Mater. **20**, 4300 (2008).
[18]A. M. Funston, C. Novo, T. J. Davis, and P. Mulvaney, Nano Lett. **9**, 1651 (2009).
[19]E. Hao and G. C. Schatz, J. Chem. Phys. **120**, 357 (2004).
[20]K. H. Su, Q. H. Wei, and X. Zhang, Appl. Phys. Lett. **88**, 063118 (2006).
[21]Y. Kurokawa and H. T. Miyazaki, Phys. Rev. B **75**, 035411 (2007).
[22]M. Kuttge, F. J. García de Abajo, and A. Polman, Nano Lett. **10**, 1537 (2010).
[23]H. T. Miyazaki and Y. Kurokawa, Phys. Rev. Lett. **96**, 097401 (2006).
[24]L. Qin, S. Zou, C. Xue, A. Atkinson, G. C. Schatz, and C. A. Mirkin,

Proc. Natl. Acad. Sci. U.S.A. **103**, 13300 (2006).
[25]B. P. Joshi and Q. H. Wei, Opt. Express **16**, 10315 (2008).
[26]B. Joshi, A. Chakrabarty, and Q. H. Wei, IEEE Trans. Nanotech. **99**, 1 (2010).
[27]P. B. Johnson and R. W. Christy, Phys. Rev. B **6**, 4370 (1972).
[28]J. Rivnay, L. H. Jimison, M. F. Toney, M. Preiner, N. A. Melosh, and A. Salleo, J. Vac. Sci. Technol. B **26**, 1454 (2008).
[29]S. I. Bozhevolnyi and T. Sondergaard, Opt. Express **15**, 10869 (2007).